Heliyon 10 (2024) e32448

Contents lists available at ScienceDirect

Heliyon

journal homepage: www.cell.com/heliyon

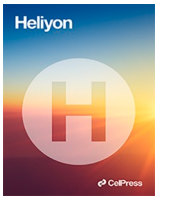

Research article

Synthesis, characterization and evaluation of new anti-inflammatory iron charge transfer complexes

Mervette El Batouti [a], E.H. El-Mossalamy [b], Nouf Al-Harby [c,*], H.A. Fetouh [a]

[a] Chemistry Department, Faculty of Science, Alexandria University, Egypt
[b] Chemistry Department, Faculty of Science, Benha University, Benha, Egypt
[c] Department of Chemistry, College of Science, Qassim University, Buraydah, 51452, Saudi Arabia

ARTICLE INFO

Keywords:
Donor
Acceptor
Charge transfer
Computational
Biological activity
Anti-inflammatory

ABSTRACT

The novelty and the essential purpose of this research is the preparation of new anti-inflammatory iron complexes in water green solvent using critical micelle concentration of anionic surface active agent (SAA). Three new anti-inflammatory iron complexes have been prepared. Thiophene-electron **(es)** donor (D) Schiff base (2-(2-OH-benzylidene)-amino)-4, 5, 6, 7-tetrah ydrobenzo[b] thiophene-3-carbonitrile) has been prepared. Molecular structures of all samples were confirmed based on CNH analysis, ^{1}H NMR and ^{13}C NMR spectra. The molecular structure of Schiff base is further confirmed by computational chemistry using the DFT-B3LYP method, 6-31G (d) basis set. Observed and simulated ^{1}H NMR, UV–Vis. IR/Raman spectra confirmed the molecular structure of D. This Schiff base is intercalated to ferric chloride ($FeCl_3$) giving pure iron charge transfer complex (CTCs). *In vitro* and kinetic studies confirmed Fe-CTC complexes had (concentration-dependent) potent antimicrobial-, good anti-inflammatory activities. Free radical scavenging activity nitrous oxide ($NO^{\cdot}$) of Fe (III)CTCs is attributed to geometry Fe(III) ions as distorted octahedral (either monoclinic or triclinic single crystals) *via* functional groups (-C]N–O, NH_2). Elemental analysis and EDS spectra confirmed strong binding between iron and hetero atoms (N, S, O) of D molecules.

1. Introduction

CTCs of Schiff bases: exhibited various medicinal and biological activities such as antibacterial; solid electrolytes for batteries and fuel cells; Formed *via* electron transfer from es-D to an es-acceptor; rich in electron (es) density. Anti-inflammatory, analgesic, anti-cancer, antidepressant and antimicrobial activities are not widely reported for CTC.

Inflammation is a physiologic defense mechanism of human body against infection by burns, toxic, carcinogenic chemicals and allergens. Severe inflammation is an etiologic factor for chronic illnesses. Nowadays, due to the wide spreading of pathogenic microorganisms, developing new anti-inflammatory compounds with few side effects is a must [1,2].

Low concentration NO in is a bio regulatory molecule in the human body; it physiologically affects blood pressure, transduction of neural signals and platelet function. NO as ADPH-dependent enzymes–NO–synthases break terminal N-atom guanido of L-arginine amino acid (aa) [3]. During infections and inflammations, NO released in-vivo rapidly and negatively impacts the human body [4].

Many metal complexes are anti-inflammatory [5,6]. However, these complexes showed many drawbacks, such as toxicity for red

* Corresponding author.
E-mail address: Hrbien@qu.edu.sa (N. Al-Harby).

https://doi.org/10.1016/j.heliyon.2024.e32448
Received 12 January 2024; Received in revised form 1 June 2024; Accepted 4 June 2024
Available online 8 June 2024

blood cells [7]. Cu(II) complex is thirty times more efficient than anti-inflammatory aspirin antibiotics. Intercalation Cu(II) ion to non-*anti*-inflammatory salicylate induced anti-inflammation activity [8].

Anti-inflammatory monoamine oxidase (MAO) A, and B isoforms oxidize dopamine have seventy percent aa identity and contain 527aa and 520 aa respectively. Either MAOA or MAOB have unique substrates (S), inhibitors (I), location in living cells and gene expression [9,10]. MAOA has S: serotonin, adrenaline and noradrenaline; irreversibly inhibited by little concentration of clorgyline. Defects cause depression and abnormal aggressiveness. MAOB acts on β-Ph.-ethyl- and benzyl-amine, reversibly inhibited by low-concentration deprenyl that enhances neuron-protection [11,12]. Its neural expression increases in elderly people causing disorders such as Alzheimer's-, and Parkinson's disease. N–CH_3-2-Ph-maleimide-de-H-epiandrosterone, berry fruits anthocyanin, adole and benzo-furans are inhibitors to both forms MAOA and MAOB [10,13].

Inflammation causes pathogenic cascades of neuro-degeneration. Chemotherapy retards disease progress [14,15]. Accumulated intracellular abnormal proteins trigger the production of inflammatory mediators. Inflammatory is an immunity response removing diverse insults to remove damaging agents that increase the level of cyclooxygenase 2 (COX-2) in the brain [16,17].

Most of the reported iron complexes lacked computational analysis [18–22]. In this current study, computational chemistry predicted the physicochemical properties of Schiff base ligand to iron complexes. Density Functional Theory (DFT/B3LYP/6-311+G (d, p)) basis set enabled calculation various parameters of molecular structure such as absorption spectra: UV–Vis., FTIR, and 1H and 13CNMR, energies of frontier molecular orbitals HOMO, LUMO to confirm experimentally observed spectra, atomic charges, dipole moment in solvent continuum, non-bond orbital (NBO) and thermodynamic properties, vibrational band, nonlinear optical (NLO) activities [23].

Agreement between experimental and simulated data confirmed the molecular structure, electronic and spectroscopic properties for various Schiff base and related CTCs [24,25].

Biologically active Fe complexes are neuro protectors inhibited acetyl-, and butyryl cholinesterases (BuChE) [9] *via*: interaction with calf-thymus DNA (binding: nucleo bases and blood serum albumins (SA) (the predominant proteins [A&B] control transport drugs and small molecules (fatty acids, metabolites, etc. in blood circulation to target cells [17–20]. Fe (III)-NSAID complexes are potent microbiologically active than corresponding free NSAIDs therapeutic drugs [18[, Fe complexes have a good selectivity index and are efficient for severe Alzheimer disease (AD) [22]. Many transition metal CTCs are reported as antimicrobial agents; however, evaluation of anti-inflammatory activities of these hybrid organic materials is lacked in the literature.

Some Fe complexes are anti-inflammatory. The scavenging activity of octahedral $Fe(III)_2$ cephradine is due to the bridging coordination of 2 Fe(III) ions with the ligand in a stable five membered ring. The first Fe (III) ion is coordinated to the carboxylate group and the adjacent nitrogen atom with a stable five membered ring. The second Fe(III) ion is attached to nitrogen atom of –C]N–O group and NH_2 with a stable five membered ring.

This study aims to prepare new CTCs for potential applications as antioxidant and anti-inflammatory agents. The originality of this work is the preparation of such low-cost new anti-inflammatory Fe-CTC in green water solvent. Chelation of iron to thiophene Schiff base (D) has not been reported yet. Iron is necessary for all biological functions of the human body. CTC enabled a large loading capacity of iron with a low dose of organic ligand (CTC) that carries benzene rings like another antibiotic. The large loading capacity of iron on a small dose of organic ligand decreased the cytotoxicity of such iron-CTC on normal human cells.

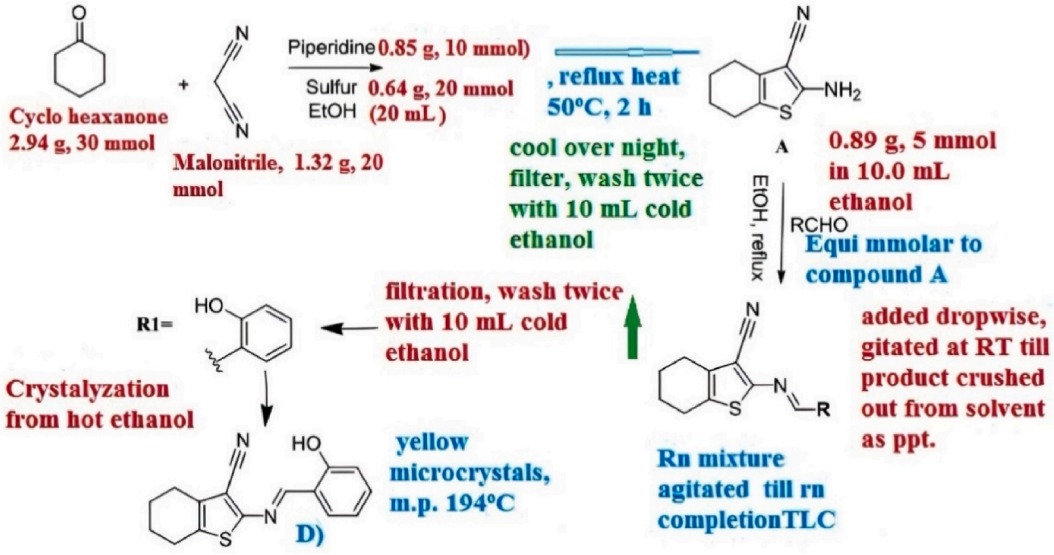

Scheme 1. Preparation scheme of Thiophene Schiff base.

2. Experimental

Chemicals in this study have high purity obtained from Sigma Aldrich Co. Both Schiff base (es D) and corresponding Fe-CTC samples have been prepared using the modified method reported elsewhere, Scheme 1 [23].

Solid CTC samples of different molar ratios have been prepared by mixing: 1 mmol Fe (III) chloride dissolved in 25 mL double distilled water. Volumes: 5 mL, 10 mL and 15 mL $FeCl_3$ have been added to 10 mL (1 mmol) Thiophene Schiff base in batch mode experiment. 10 mL 0.1 M Na dodecyl sulphate anionic surfactant was added to each reaction mixture to solubilize all constituents. Each mixture was refluxed and heated for 20 min at 35 °C. Solvent water is slowly evaporated at ambient temperature, followed by filtration. Solid Fe-CTC samples are washed with a water-ethanol mixture, collected and dried under vacuum over anhydrous $CaCl_2$ for 24 h [23]. The new preparation method was confirmed as good yield 90 % obtained in each trial. The purity of each complex sample is confirmed using thin layer chromatography on Baker-Flex silica gel 1B–F plates. All samples showed one spot using eluent 1:3 v/v ethyl acetate-normal hexane, each spot is measured at specified wavelengths using a scanner in absorbance/reflectance mode [24,25].

To confirm the molecular structure of Fe-CTC, elemental microanalysis analysis (C, H, and N) of dry pure samples was carried out using CHNS-932 (LECO) Vario elemental analyzer. Inductively coupled plasma/optical emission spectrometry (ICP/OES) is used to determine wt.% of Fe (III) ion in the test sample after digestion in conc. HNO_3 to remove all organic matter and leaving only metallic residue, Table 1.

Elemental composition of the tested samples suggested the bonding mode in solid Schiff base -Fe CTC can be represented as in Scheme 1.

Sulphur (S) atom is the main chelating agent and it enhanced biological activity of Fe CTCs samples.

Mass spectra are recorded using Thermo Scientific GC-MS analyzer Instrument at 70 eV for es ionization; Nuclear magnetic resonance ^{1}H, ^{13}C NMR were recorded using Bruker spectrometer (400 MHz, DMSO-d_6). Chemical shift (δ ppm) is taken relative to internal standard TMS.

Fe CTCs are stable, soluble in polar solvents and insoluble in organic solvents. Molar conductivity for FeCTC1 (5.2 S cm^2 mol^{-1} for 1.0 mM DMSO solution). Low molar electrical conductivity (ΛM) may indicate non-electrolytic nature. On the other hand, FeCTC2, $FeCTC_3$ showed ΛM values in the range (65–70 Scm^2mol^{-1} such as uni uni valent electrolytes [1].

Physicochemical parameters for Fe-CTC3 samples evaluated by recording UV–Vis. spectra using JASCO V-530 UV–Vis. Spectrophotometer; IR spectra using Buck scientific 500-IR spectrophotometer (KBr disk). Raman spectra using Senterra Raman spectrometer. Raman shifts of powder samples deposited on glass slides at room temperature were analyzed to ensure sample uniformity. Laser λexcitation 532 nm, scan range: 3700-100 cm^{-1}, 100 mW, 4 cm^{-1} resolution and 25 accumulative scans. Powder X-ray diffraction pXRD patterns at 25 °C at range 2-theta (θ) 5°-70°, 0.01° step, 1° per min using Cu-Kα radiation λ 1.5418 Å at 40 kV acceleration, Bruker D8 advance diffractometer. Intensity (a.u.) of reflected X-rays plotted versus 2θ° [2]. Atomic percent determined from EDS spectra recorded using Oxford Inca X-act detector, EDS-SEM, 15 kV for chemical analysis [13].

Thermal analysis (TGA and DTA) was measured using Shimadzu TGA-50H computerized thermal analyzer, heating rate 10 °C $min.^{-1}$ under N_2 flow rate 20 mL $min.^{-1}$, α-alumina powder DTA standard material [26].

Antimicrobial activity: bacteria/fungi were cultured in solid broth media. Isolated microorganisms (MO) colonies were selected. Mueller-Hinton agar is the preferred growth media. Filamentous fungi and yeasts were tested using standard M38-A and M44-P methods respectively. Response to antifungal agents recorded using disc diffusion standard method. Plates inoculated with^{+} bacteria: *S.aureus* and *B.subtilis*; G^{+} bacteria: *E.coli* and *P.aeuroginosa* incubated 24 h at 37 °C. Fungi *C. albicans A. flavus* were incubated for 48 h at 25 °C. Ampicillin antibacterial antibiotic (Ab) and amphotericin antifungal Ab are positive controls respectively. Filter discs impregnated with 10 μL solvent (distilled water, chloroform, DMSO) negative control). Blank paper disks with 8.0 mm diameter impregnated 10 μL test concentration sample. The sample diffuses from the disc to the surrounding agar. The solubility and molecular size of the sample determine the infiltration area. Inhibited MO on agar not grow in clear zone area. Diameters of inhibition zones (IZ) is measured in mm [26].

Anti-inflammatory activity is measured: 20 μL, 10 m MNa–NO_2–prusside was mixed with 5 μL phosphate buffer, volume (μL) 2, 3, 5, 6, 8, 10 test sample FeCTC, incubated at 25 °C, 2.5 h. 20 μL Griess reagent (1g sulphanilic acid + 0.1g naphthyl-ethylene diamine.2HCl) was added to the mixture, left stand 30 min at room temperature, Absorbance was read at 540 nm [7,8].The scavenging activity was calculated using equation (1).

$$\text{Nitric oxide scavenging activity} = \frac{A_{control} - A_{sample}}{A_{control}} \times 100 \quad (1)$$

Quantum chemical calculations of D molecules employed using Gaussian 09 program: DFT, B3LYP method at 6-31G (d) basis set.

Table 1
Elemental analysis of weight percent of thiophene Schiff base and Fe-CTCs.

Sample	Wt.%			
	C	**H**	N	Fe
Thiophene Schiff base (D)	50.11	3.08	11.88	–
Fe-CTC1	52.3	3.13	12.69	12.3
Fe-CTC2	54.60	5.43	14.9	13.71
Fe-CTC3	65.25	6.86	16.74	15.6

Minimum energy concerning nuclear coordinate(s) for unconstrained optimized geometry (predicted electronic transitions and interpreted observed UV–Vis. absorption spectra. Relaxation geometrical parameters are simulated till reaching full convergence criteria without constraints except dihedral angles retaining 2D structures. Equilibrium geometries with true minima harmonic vibrational frequencies were calculated in DMSO using the PCM model [25]. ^{1}H NMR (δcalc, ppm) was calculated (at obglobal minimum geometry) using GIAO approximation. ^{1}H absolute isotropic shielding (σi, ppm) parameters converted into ^{1}H NMR (δ_{calc}, ppm.) = σ_{TMS} - σ_i [23].

3. Results and discussion

Fig. 1 showed mass spectra (relative abundance versus (mass/charge) ratio for defragmented ions) showed molecular weight (Mw. g mol^{-1}) of D and FeCTCs respectively as the molar mass of the last ion peak.

Mw: Fe-CTC1 (662.38), Fe-CTC2 (758.57) and Fe-CTC3 (834.65).

EDS spectra showed the main atomic % are C, Fe, S and O confirmed the inclusion of all elements of D into FeCTCs. Polarizable S atom is the favorable chelation site to Fe according to hard soft acid base principle.

^{1}H NMR (Intensity versus chemical shift (δ, ppm) spectra confirmed the number of protons, Fig. 2:

δ: 9.0 (1H singlet, OH 9.98 (1H singlet, –CH]N) 7.80–7.07 (4H multiple, aromatic Hs)

The number of protons of thiophene Schiff base maintained in CTC and additional signals at higher δ ppm have been observed ^{1}HNMR became broad on both CTC formation and complexation to iron. All these observations confirmed the molecular structure of the prepared samples.

Fig. 3 showed ^{13}C NMR (intensity versus chemical shift (δ, ppm) spectra) of Schiff base (100 MHz, DMSO-d_6) δ_C 40; 40; 56; 110; 118; 125–130; 136–144) maintained in all ^{13}C NMR of CTC and Fe-CTCs [23].

Noise in ^{13}C NMR spectra as Schiff base (electron donor ligand binding Fe forming FeCTC intercalation complexes have various

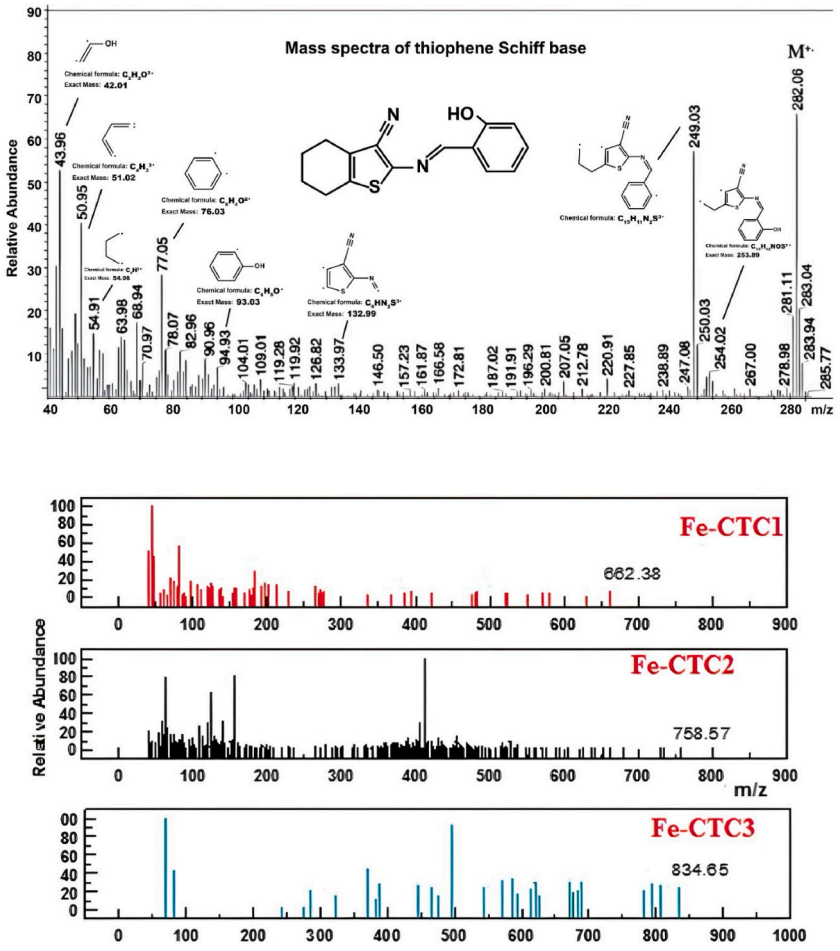

Fig. 1. Mass spectra of thiophene Schiff base and FeCTCs

Fig. 1 (continue) showed EDS spectra (counts versus binding energy (eV).

Fig. 1 (continue):EDS spectra of FeCTCs.

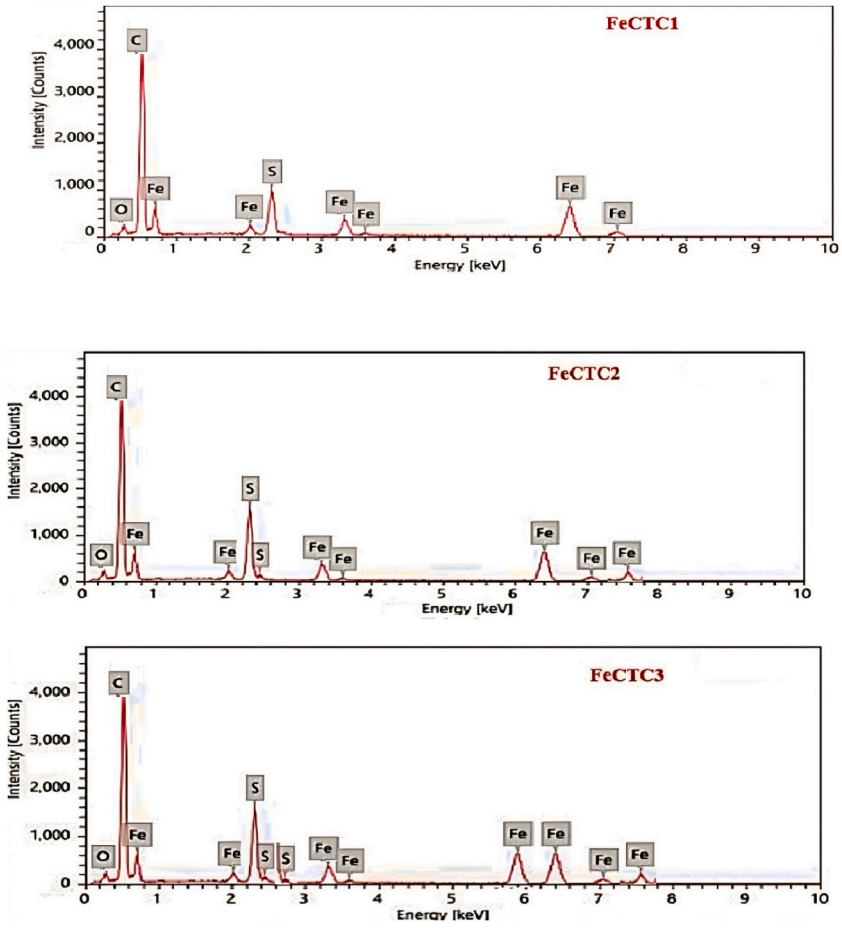

Fig. 1. (*continued*).

environments around carbon atoms in each sample.

Fig. 4 showed indexed pXRD patterns of FeCTCs. Sharp diffraction peaks indicated good crystaline samples. Trend of lattice planes and crystallinity increased in the order:

FeCTC1 > FeCTC2 > FeCTC3

FeCTC1 crystalized in monoclinic unit cell. The latter two complexes in triclinic, Table 2.

Good crystallinity of CTCs confirmed good purity and long range storage time without spoilage on aging [27].

Central iron ion arranged in distorted octahedral crystalline with iron-oxygen (Fe–O) bond is the shortest bond distance.

FeCTCs interaction with DNA (biomolecule target for therapeutic drugs *via*: inhibition nucleotide synthesis& topoisomerase and blockage DNA replication. Labile ligands in metal-based drugs (e.g., cisplatin) offer vacant coordination sites for covalent binding DNA-bases, Scheme 2.

From UV–Vis. spectra for FeCTC3 sample dissolved in ethanol at 25 °C represented in Fig. 5, Spectral physical parameters: formation constant (K_{CT}), standard free energy ($\Delta G^{\circ}_{complexation}$), transition dipole moment (μ), oscillator strength (f, arbitrary unit expressed transition probability of CT band), ionization potential (I_D) were calculated using equations (2)–(8) [23], Table 3.

$$f = 4.319 \times 10^{-9}\left(\varepsilon_{max} \cdot \Delta\upsilon_{1/2}\right) \tag{2}$$

Where ε_{max} maximum extinction coefficient of CT band corresponds to half-bandwidth $\Delta\upsilon_{1/2}$, cm^{-1}.

$$\mu_{(Debye)} = 0.958\left(\frac{\varepsilon_{max} \cdot \Delta\upsilon_{1/2}}{\upsilon_{max}}\right)^{1/2} \tag{3}$$

μ signifies allowed ππ*transition provided nonzero transition dipole moment.

$$I_{D(eV)} = 5.76 + 1.53 \times 10^{-4} \cdot \upsilon_{CT} \tag{4}$$

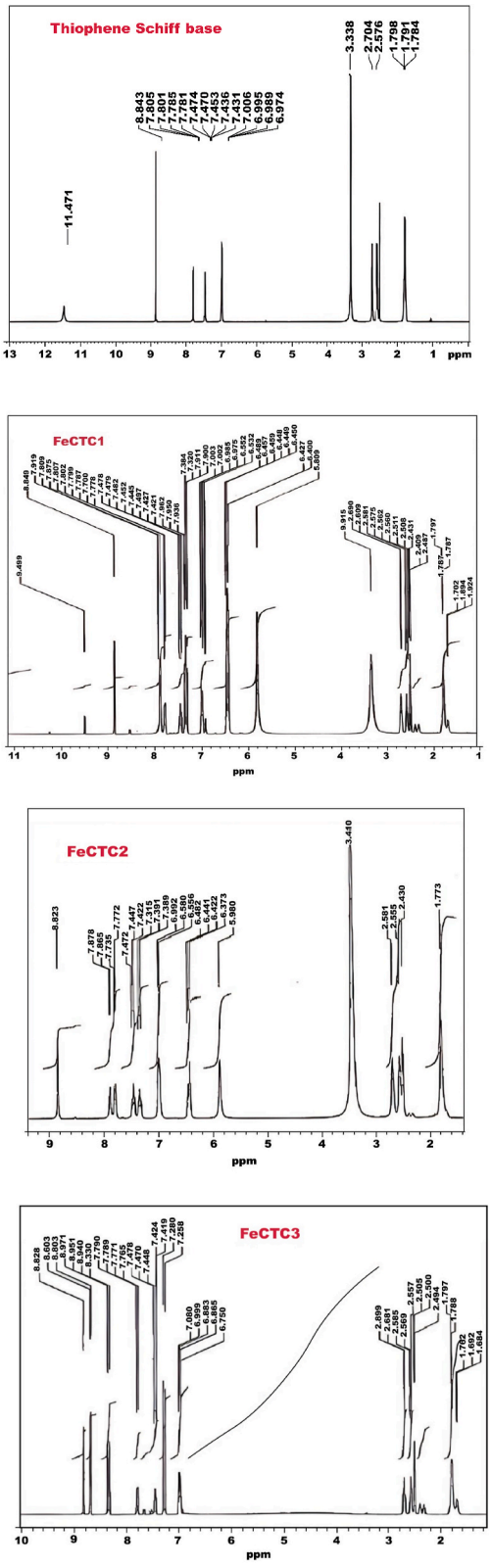

Fig. 2. H NMR spectra.

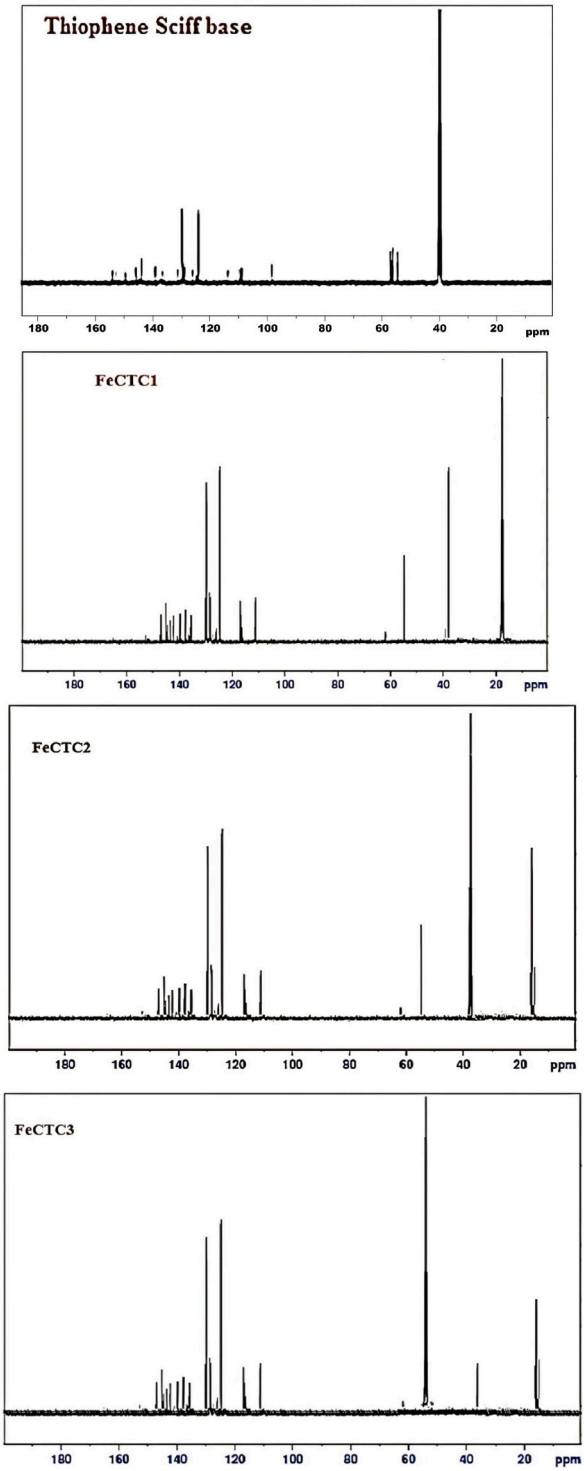

Fig. 3. ^{13}C NMR spectra.

Where wavenumber υ_{CT}, cm^{-1} corresponds to *CT* band of D-Fe interaction. es- Donation is measured by I_D energy required to remove es from HOMO to LUMO energy levels.

Energy of dissociation (W) calculated from the corresponding CT energy (E_{CT})) I_P and electron affinity (E_A):

$$E_{CT} = I_P - E_A\ (0.64\ eV) - W \tag{5}$$

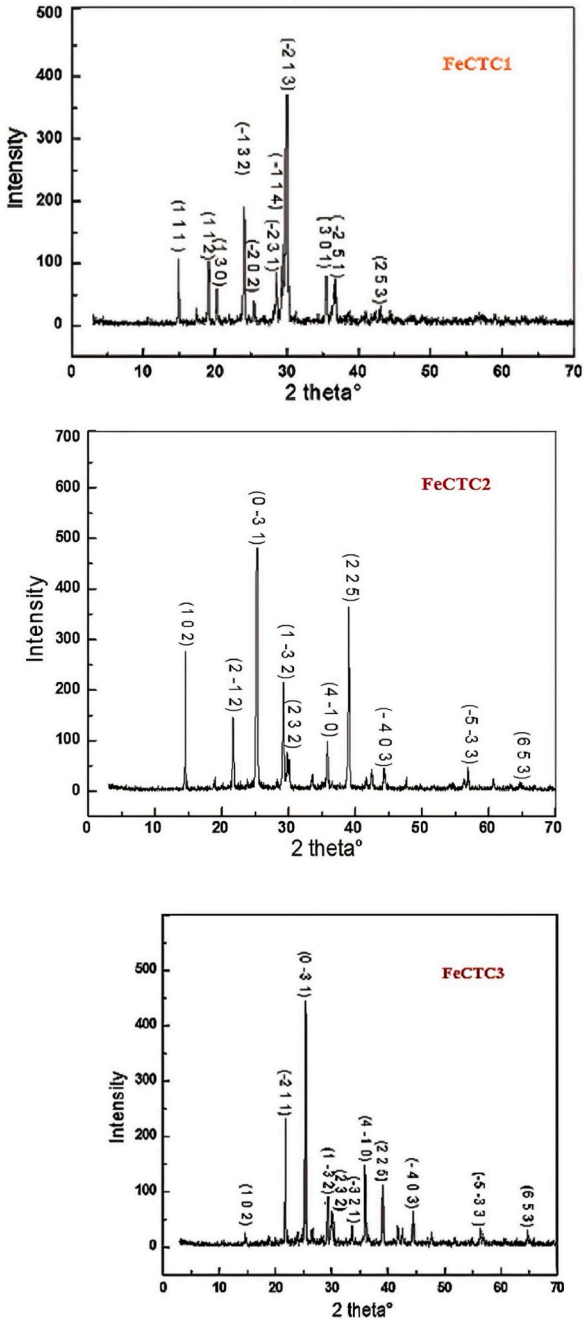

Fig. 4. pXRD patterns of FeCTCs.

Table 2
Crystalline parameters.

Sample	FeCTC1	FeCTC2	FeCTC3
pdF card	1505763	4342413	
Crystal System, Space group	Monoclinic, P 2_1	Triclinic, p1_2	
Lattice parameter (Å): a, b, c,	7.90, 16.00, 13.10	10.80, 11.02, 12.90,	
	$\alpha = \gamma$ 90°, β 94.60°	α 89.00°, β 77.61°, γ 85.00°	
Volume (Å^3)	1538.79	1792.50	

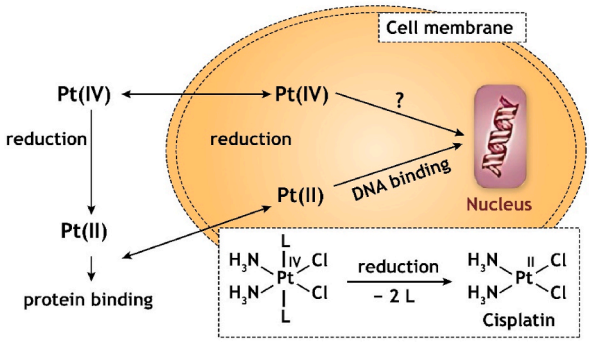

Scheme 2. Mode of interaction: cisplatin –DNA binding.

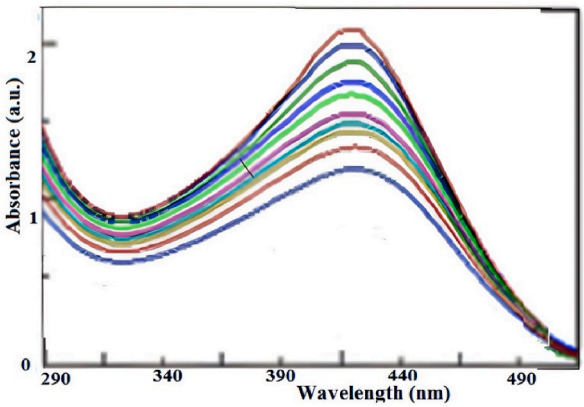

Fig. 5. UV–Vis. Absorption bands of FeCTC3 at different molar concentrations increasing upward.

Table 3
Spectroscopic and physical parameters of Fe-CTC3 complex.

$\lambda_{max.}$, nm	I_D, eV	K_{CT}, $Lmol^{-1} \times 10^4$	ε_{max} L $mol^{-1}cm^{-1}$	E_{CT}, eV	μ(D)	W, eV	RN	$-\Delta G^o \times 10^5$
429	13.31	5.38	1.34	3.2	111	6.44	0.34	9.1

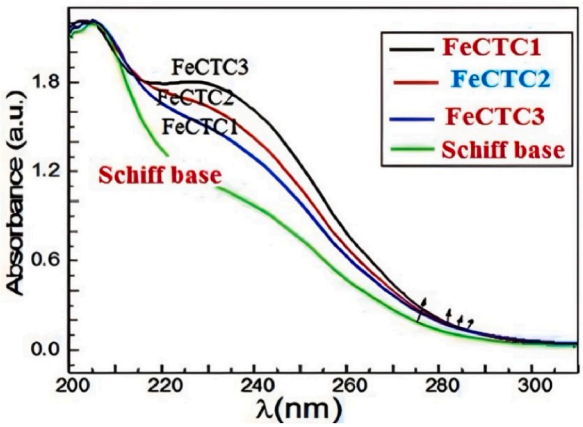

Fig. 6. (Continue): UV-absorption spectra of Thiophene Schiff base and FeCTCs.

Energy of resonance (R_N) in ground state (contributes to stability constant) determined using the relation:

$$E_{CT} = 7.7 \times 10^{-4} / [h\nu_{CT} / [R_N] - 3.5] \quad (6)$$

Where Energy (E_{CT}) of D-Fe: $\pi\pi^*$ interactions calculated using eq. 7

$$E_{CT} = (h\upsilon_{CT}) = 1243.667 / \lambda_{CT(nm)} \quad (7)$$

Where $\lambda_{CT\ band}$. $\Delta G^o_{complexation,\ 25}$ (kJ. mol.$^{-1}$) calculated using the equation:

$$\Delta G^o_{complexation} = -2.303RT\log K_{CT} \quad (8)$$

Where R 8.314 J mol.$^{-1}$ K^{-1}), absolute temperature and K_{CT} is formation constant of CTC (L mol^{-1}.).

The optical activity of Fe-CTC confirmed by UV-spectra in DMSO, Fig. 6. The intense absorption bands at 220–240 nm confirmed electronic transition.

Absorption bands at range 285–297 nm confirmed interaction of FeCTCs with DNA into stable FeCTC-DNA adducts. Chelating ligand D stabilized FeCTCs for enhancing non-covalent binding to DNA. Example, chemical linkages to grooves, electrostatic interaction and altering chemistry of nucleo bases. Band positions affected by ligand crystal field [19–23].

High negative $\Delta G^o_{complexation}$ indicating spontaneous exothermic Thiophene Schiff base-Fe interaction with high probable CT transitions [23].

TGA and DTA thermo-gram reflect the thermal stability of tested samples, Fig. 7.

Thiophene Schiff base decomposed gradually from 14.0 g to 8.0 g at 590.4 °C. DTA thermogram showed one exothermic and endothermic peaks due to dehydration and carbonaceous residues, respectively [26].

Molecular geometries of D optimized, Fig. 8. Calculated structural parameters are collected in Table 4. Dihedral angles $C_7N_6C_5C_2$ -35.3°, C7N6C5S4 29° ensured non-planar benzene rings against thiophene ring. Bond lengths and angles calculated for numbered atoms were compared with observed values for similar groups in different compounds using es-diffraction and microwave spectra of phenol. pXRD patterns of different Schiff bases. Proposed vibrational assignments based on those estimated from QM calculations [25].

For ^{1}H NMR spectra cal., observed ^{1}H δ assigned to corresponding Hs, Table 5. Strong singlet at 3.34 ppm (inherent water (D–O–H) in DMSO-d_6. Singlet at 11.47 ppm (OH (H_{25}) diminished in D_2O by H-D magnetic exchange. The predicted δ of the OH proton differ from $\delta_{observed}$ due to de-shielded HB interactions. CH]N proton (olefin downfield sp^2 C–H): observed singlet at 8.84/8.41 ppm; H_{15}/H_{11}) agreed with δcal. at 8.97/8.73 ppm. Aromatic $H_{22\text{-}25}$ predicted at δ 6.89–7.92 ppm (observed singlets at 7.79 and 6.99 ppm, doublet at 7.47, 7.45 ppm. Downfield shift of H_{27}/H_{21}, H_{28}/H_{22}, H_{33}/H_{27} and H_{34}/H_{28} attributed to nearer thiophene conjugation. After exclusion $\delta_{calc.}$ OH-proton, High R^2 0.997 was obtained between calc., exp. ^{1}H NMR δ [23].

Fig. 9 showed observed and simulated IR and Raman bands spectra Major contribution for normal vibrational modes at calculated frequencies was predicted from atomic displacements visualized using Gauss View program. Observed and calculated wavenumbers, $\overline{\upsilon}$ assigned, Table 6.

Optimized geometry predicted excitation energy (E_{exc}), (λ_{max}, nm), (f) and major electronic transitions obtained from a log file using GaussSum-2 0.2.0 program), Table 7. Wave function (FMOs: HOMO and LUMO were sketched in Fig. 10. Simulated electronic absorption UV–Vis. spectra in DMSO. Obs. band at λ_{max}.400 nm corresponds to the transition from the ground state (S0) to the first excited state (S1) with a probability ninety-eight percent, agreed with the predicted value at $\lambda_{max.cal}$ at 408 nm with the highest (f) 0.6044. HOMO wav function localized on bonding π orbitals of azo group (π N_7]C_6), aromatic (π C_{10}]C_{11}, π C_8]C_{13}), thiophene (π C_1]C_3, π C_2]C_5) rings and N-NBO. Anti-bonding π* orbitals: azo group (N_7]C_6), aromatic (C_{11}]C_{12}), ring (π* C_2]C_5), S0→S2 T.S. (HOMO-2→LUMO; 97 %) calc. at 341 nm strongly matches the third observed absorption peak at 345 nm. The electronic absorption peak observed at 294 nm coincides with $\lambda_{calc.}$ 299 nm: S0→S3 transition (HOMO-1→LUMO; 96 %). HOMO-1 is characterized by π orbitals aromatic ring (π C_9]C_{10}, π C_{12}]C_{13}) and O-NBO. Oscillating strength (0.69) LUMO+2 is represented by anti-bonding π* orbitals of

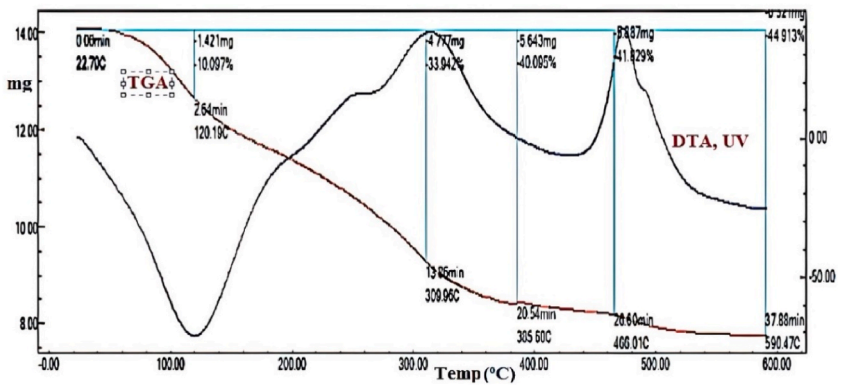

Fig. 7. TGA and DTG thermogramms of thiophene Schiff base.

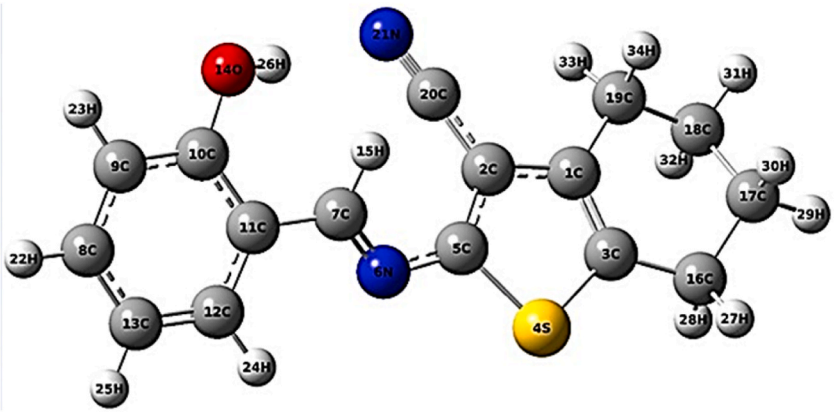

Fig. 8. Optimized structure of Schiff base according to naming priority.

Table 4
Calculated structural parameters for Schiff base compared to observed parameters for similar structures.

Parameters	Electron Diff.	Mw	X-ray				b
	c	d	e	f	g	h	
rC_1C_2						1.436	1.419
rC_3S_4				1.728	1.746	1.729	1.659
rC_5N_6[a]				1.386	1.379		1.373
rC_7N_6[a]				1.281	1.283	1.287	1.293
rC_1C_{19}					1.500		1.526
rC_1C_{15}					1.500		
$r^aC_1C_3$					1.366		1.368
$r^aC_{20}N_{21}$				1.132	1.138	1.132	1.167
$r^aC_{18}N_{19}$				1.132	1.138	1.132	
$r^aC_7C_{11}$					1.452	1.449	1.451
$\Delta_{rC12C13\ phenol}$	1.399	1.40					1.395
$r^aC_{10}O_{14}$	1.379	1.39		1.360		1.354	1.363
$r^aO_{14}H_{26}$	0.958	0.96					0.973
rC_8O_9			1.369				
rC_8C_{16}			1.348				
$r^aC_{17}C_{16}$			1.408				
ΔrC.H cyclohexane							1.098
rC_7H_{15}							1.093
rC_7H_{11}							
ΔrC.H phenol	1.086	1.09					1.086
$\angle C_1C_3S_4$					112.4	110.8	111.0
$\angle^a C_3S_4C_5$				91.8		91.0	92.1
$\angle C_{16}C_{17}C_{18}$ cyclohexane							115.5
$\angle C_{19}C_1C_3$					124.0		123.9
$\angle C_{10}C_{11}C_{12}$ phenol	120.2	120.					120.0
$\angle C_{11}C_{10}O_{14}$	121.2	122.				122.7	120.1
$\angle^aC_{10}O_{14}H_{25}$	106.4	109					112.2
$\angle C_{17}C_8O_9$			109.1				
$\angle^aC_{10}O_9C_8$			105.8				
$\angle C_8C_{17}C_{16}$			107.1				
$\angle^a C_7N_6C_5$				121.2	118.9	120.0	118.8
$\angle^aN_{21}C_{20}C_2$				177.8		179.3	176.9

[a]bond distances (r, Å, bond angles ∠ °.
[b] for structure, atom numbering.
[c, d] Electron diffraction and microwave structure of phenols respectively; e-h XRD patterns + pdF cards phosph alkene thiophene derivatives, 2-salicylidene–NH_2–4-7-tetra-H-benzo[b] thiophene-3-carbonitrile (CN), 4-7-tetra-H-1-benzothiophene-3-CN, azomethine dye: 2-((2-OH-3-OCH_3-Ph-NH)methyl)-4-Ph-thiophene-3-CN [24].
[a] Structural parameters were averaged except those with asterisks.

nitrile group (π* $N_{18}\hat{}C_{19}$) and S-NBO. Simulated UV–Vis. spectrum resemble exp., $\Delta E_{LUMO\text{-}HOMO}$ 3.515eV, respectively. Low value explains that D molecule is soft polarizable Schiff base PA [23]. Fig. 11 should multiple density of states of Schiff base (DOS) confirmed high delocalized electron density.

Luminescence properties of CTC ground-or excited-state (photo induced) tautomerism *via* excited state intra-molecular proton

Table 5
Experimental and calc.^{1}H NMR shifts δ (ppm) of D.

Atom NO.	Δexp.	δcal.
H_{15}	8.84	8.97
H_{27}, H_{28}	2.70	2.68
H_{33}, H_{34}	2.58	2.64
H_{29}, H_{30}	1.79	1.85
H_{31}, H_{32}	1.78	1.81
(R^2) between δexp, δcal.[a]	0.997	

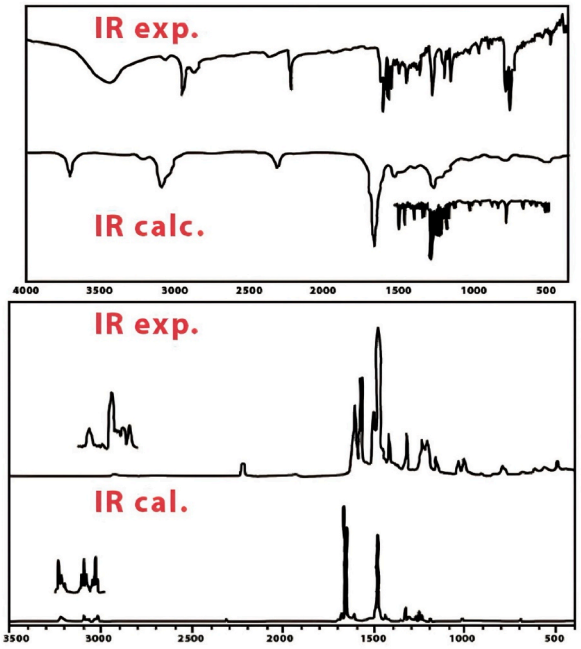

Fig. 9. Simulated and observed IR and Raman spectra of thiophene Schiff base.

transfer (ESIPT) can be triggered by solvents or photo excitation elevate the optical activity based. Emission spectra based on enol = keto equilibrium.

Large oscillation strength (f) 0.6 indicating the most probable transition is $S_0 \rightarrow S_1$ transition based on required ionization energy. Contributions less than 10 % were omitted, all T.S. are singlet-A symmetry.

Antibacterial and antifungal activities of Ds and Fe CTC against six pathogenic microorganisms (two G^+, two G^- bacteria and two fungi are included in Table 8:

Some Fe CTCs showed high good antimicrobial activities against *S. aureus*, IZ (mm) 29, 27, 24, respectively compared with Ab (21 mm), Moderate antibacterial activity against B. subtilis:26, 24, 26 (Ab 26 mm)]. FeCTC1 showed the highest antibacterial activity against P. *aeruginosa*, IZ 29 mm (Ab 26 mm). The activity of other CTCs against E. coli, P. *aeruginosa* was relatively less than Ab. CTC showed moderate activity against *C. albicans*, IZ 14, 14, 15 respectively (Ab: 19 mm). Thiophene Schiff base D showed no antimicrobial, CTC (D-Fe) interaction in FeCTC increased biological activity against the same microorganisms.

Reduction of NO radical by therapeutic anti-inflammatory complexes, maximum NO-scavenging activity evaluates anti-inflammatory [3]. Fe-CTC exhibited well NO scavenging activity107.01, 130.00, and 149.20 respectively in comparison with erythromycin (E) antibiotic (Ab) 65 %, Fig. 12. So, Fe-CTCs can be suggested for application in vascular regulation, improving immune response and preventing cell apoptosis [4. 23].

Fe-CTCs are anti-inflammatory agent stabilizing lysosome membrane and limiting inflammatory response *via* preventing lockage constituents of activated neutrophil as bactericidal enzymes and proteases catalyzing inflammation and damage upon extra cellular release [13]. Scavenging activity of FeCTCs to NO means similar activity to OH and other scavenging ROS.

The mechanism of antimicrobial activity of FeCTC: penetration cell membrane of microbes, binding and cleavage DNA and activating nuclease enzyme.

The antioxidant activity: Scavenge free radicals and increase in reduced glutathione level, prevent the oxidative stress, AChE and MAO-A&B. Equation (9) provided an example free radical scavenger for DPPH• into 2,2-di-Ph-1-picryl-hydrazyl

$$DPPH\bullet + AH \rightarrow DPPHH + A\bullet \quad (9)$$

Table 6
Selected Observed and calculated frequencies (cm^{-1}) of D.

Obs.		Cal.				Assign.
IR	Raman	Unscaled	scaled	IR Int.	Raman active.	
3426s,br		370	356	112	129.7	ν_{O-H}
	3097w	322	310	16	286.0	$\nu_{s\ C-H\ ar}$
	3080sh	322	310	9.0	75.05	$\nu\ _{C-H\ ar}$
	3064br	321	308	14.4	185.4	$\nu\ _{C-H\ ar}$
3051w,br	3050sh	319	3077	3.4	72.53	$\nu\ _{C-H}$ ar
	3032sh	311	300	18.7	33.06	$\nu\ _{C-H\ ol}$
2998sh	2988br	309	298	44.7	107.0	$\nu\ _{C-H\ al}$
2998sh	2988br	310	297	70.1	291.0	$\nu\ _{C-H\ al}$
2935s	2936br	305	293	22.1	19.34	$\nu\ _{C-H\ al}$
2935s	2936br	304	292	21.7	112.1	$\nu\ _{C-H\ al}$
2895sh	2902br	302	291	16.5	122.2	$\nu\ _{C-H\ al}$
2865 m	2883br	302	290	35.6	287.7	$\nu\ _{C-H\ al}$
2218s	2221w	231	222	67.7	144.7	$\nu\ _{C\ \hat{}\ N}$
1618s	1621sh	166	161	13.4	48.50	$\nu_{C=N}/\delta_{C-H}$
1599vs	1599s	166	159	423	5143	νC=N/δ_{C}−H
1562s	1567vs	163	156	30.7	98.53	ν C ····· phenol
	1531sh	161	154	45.0	341.0	ν C=C thio
1493 m	1497s	153	147	44.9	97.55	ν C ····· phenol
1442s	1473vs	152	146	44.0	54.47	ν C ····· Phenol /δ_{ip} O–H
1408w	1411s	148	142	51.1	3685	δ_{ip} C–H
1386w	1388sh	144	139	45.5	51.21	ν C ····· thio/δ_{ip} C–H
1366 m	1367sh	143	138	9.3	277.8	δ_{ip} C–H/ν C ····· thio
1315sh	1318s	139	1333	4.85	38.77	ρ CH_2
1279s		132	1267	29.86	566.3	δ O–H/ν C ····· Phenol//δ C–H
	1229 m	130	1249	6.66	148.1	δ_{twist} CH_2
1234sh	1196 m	127	1216	104.4	260.7	ν C ····· N
1194 m		124	1194	61.91	419.7	ν C ····· C_N
1147 m	1149w	121	1163	0.43	15.26	δ_{twist} CH_2
1111 m	1108sh	117	1127	0.69	3.76	δ_{twist} CH_2
1078sh		109	1045	2.26	8.45	ν C–C
1062sh		106	1020	5.01	33.97	ν C ·····
1028w	1030w	105	1005	10.23	4.71	ν C–C
	998w	998	960	8.94	106.0	ν_{as} C–S
	990sh	986	948	0.50	0.55	δ_{oop} $C-H_{ar}$
963w	945sh	964	927	2.17	2.33	δ_{oop} $C-H_{ar}$
902w	906sh	926	890	0.18	1.08	δ_{oop} CH_2
873w	870sh	879	845	1.49	9.21	δ_{oop} $C-H_{ar}$
838w	842sh	840	808	2.92	1.90	δ_{oop} CH_2
780s	779w	788	758	2.50	11.73	δ_{oop} CH_2
756vs	737sh	778	748	42.63	5.92	δ_{oop} $C-H_{ar}$
409sh	407w	407	391	16.24	2.05	τ O–H

[a]: ν: stretch; δ: bending; ρ: Rocking; γ: wagging, τ: torsion, thio: thiophen ring, hexa: cyclohexane ring.

Table 7
Calc. and observed and calculated parameters of UV–Vis. absorption spectra of D.

Trasition	E_{exc} (eV)	f	calc. λ_{max}	Major contributions[a]	Obs. $\lambda_{max.}$
$S_0 \rightarrow S_1$	3.04	0.60	408	HOMO→LUMO (98 %)	400
$S_0 \rightarrow S_2$	3.63	0.03	341	HOMO-1→LUMO (96 %)	345
$S_0 \rightarrow S_3$	4.15	0.06	299	HOMO-2→LUMO (97 %)	294

[a]DMSO solvent: PCM.
[a] HOMO−m, LUMO + n: mth orbital below HOMO, nth orbital above LUMO.

In FeCTC, Fe(III) ion binding hetero atoms N, O, S causing anti-inflammatory activity, and activate antioxidant enzymes such as superoxide dismutase (SOD), glutathione peroxidase (GPX) and catalase (CAT) that reduced activities in the affected brain region of AD patients of.

4. Conclusion

Thermally stable thiophene Schiff base is prepared in good yield from simple available precursors. The Schiff base has been characterized using both experimental and simulated spectra (UV–Vis., IR, Raman, ^{1}H NMR spectra. Both observed and calculated parameters (using DFT computational method) are in good agreement and confirm the molecular structure. Thiophene Schiff is used as

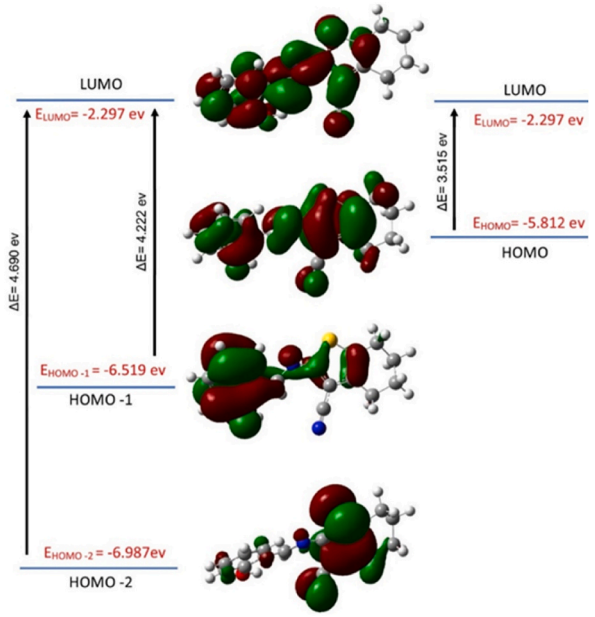

Fig. 10. Calc. energies and wave function of FMO of thiophene Schiff base.

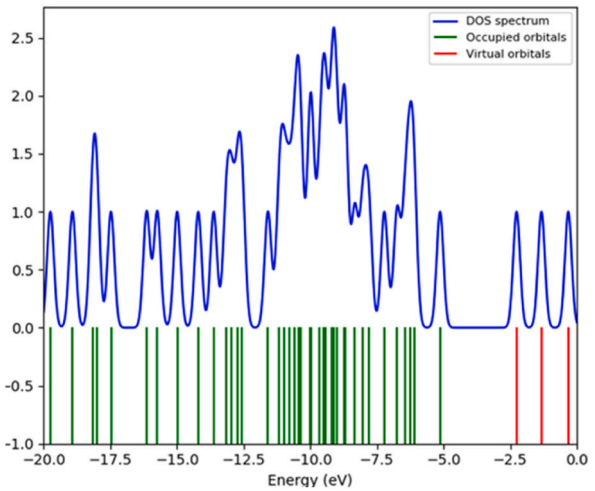

Fig. 11. Multiple DOS of d.

Table 8
IZ-diameter of G^+, G^- and fungi strains against D and Fe-CTC.

Tested sample		Inhibition zone diameter (mm/mg Sample)					
		Bacteria				Fungi	
		G^-		G^- bacteria			
		B. subtilis	*S.s aureus*	*E. coli*	*P.aeruginosa*	*A. flavus*	*C. albicans*
Control: DMSO		0.0	0.0	0.0	0.0	0.0	0.0
Standard antibiotic	Ampicillin	26	21	25	30	–	–
	Amphotericin B	–	–	–	–	17	19
Fe-CTC1		26	29	24	29	14	14
Fe-CTC2		24	27	21	28	13	14
Fe-CTC3		26	24	20	25	12	15

G: Gram reaction. Solvent: DMSO.

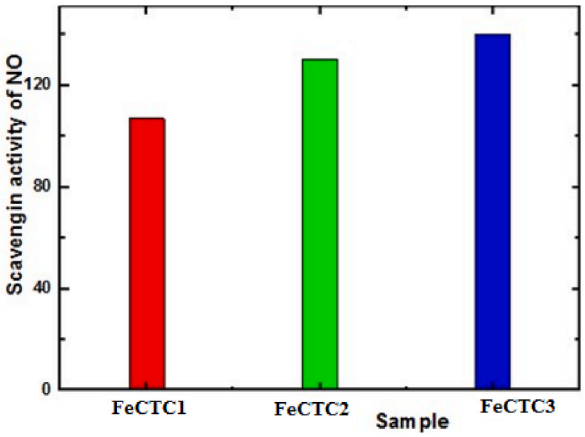

Fig. 12. Scavenging activity of FeCTCs to NO radical.

a binding ligand for Fe to yield new FeCTC with good antimicrobial activities. For FeCTCs all physicochemical parameters confirmed good optical activity. Fe-CTC is a more potent antimicrobial than Schiff bases. This finding suggested applications as biocides for diverse medicinal and pharmaceutical formulations. The promising anti-inflammatory activities of Fe CTC are attributed to multiple heteroatoms (O, N, S (especially) incorporated in the structure synergistically obtained from a combination of thiophene Schiff and Fe transition metal. Anti-inflammatory activities FeCTCs varied according to the molar ratio of Fe to thiophene Schiff base that represents new ligand for complexation of Fe to yield new biological active iron complexes.

Data availability statement

All data contained obtained in this currrent study are included in the manuscript and the supplementary materials.

CRediT authorship contribution statement

Mervette El Batouti: Writing – original draft, Methodology, Formal analysis, Conceptualization. **E.H. El-Mossalamy:** Visualization, Validation, Resources, Conceptualization. **Nouf Al-Harby:** Writing – review & editing, Investigation, Funding acquisition, Conceptualization. **H.A. Fetouh:** Writing – review & editing, Supervision, Methodology, Formal analysis.

Declaration of competing interest

The authors declare that they have no known competing financial interests or personal relationships that could have appeared to influence the work reported in this paper.

Acknowledgements

The Researchers would like to thank the Deanship of Graduate Studies and Scientific Research at Qassim University for financial support (QU-APC-2024-9/1)

Appendix A. Supplementary data

Supplementary data to this article can be found online at https://doi.org/10.1016/j.heliyon.2024.e32448.

References

[1] E. Basaran, H.G. Sogukomerogullari, R. Cakmak, S. Akkoc, T. Taskin-Tok, A. Köse, Novel chiral Schiff base Palladium (II), Nickel (II), Copper (II) and Iron (II) complexes: synthesis, characterization, anticancer activity and molecular docking studies, Bioorg. Chem. 129 (2022) 106176.
[2] Y. Deng, Q. Zhang, B.L. Feringa, H. Tian, D.H. Qu, Toughening a self-healable supramolecular polymer by ionic cluster-enhanced iron-carboxylate complexes, Angew. Chem. 132 (13) (2020) 5316–5321.
[3] A. Ally, I. Powell, M.M. Ally, K. Chaitoff, S.M. Nauli, Role of neuronal nitric oxide synthase on cardiovascular functions in physiological and pathophysiological states, Nitric Oxide 102 (2020) 52–73.
[4] M.J. Malone-Povolny, S.E. Maloney, M.H. Schoenfisch, Nitric oxide therapy for diabetic wound healing, Adv. Healthcare Mater. 8 (12) (2019) 1801210.
[5] M.N. Uddin, S.S. Ahmed, S.R. Alam, Biomedical applications of Schiff base metal complexes, J. Coord. Chem. 73 (23) (2020) 3109–3149.

[6] A.F. Elhusseiny, H.M. Hussien, H.H. Hassan, An initial demonstration of polyester monomer coordination properties: synthesis and biological activity of metal complexes derived from a new nanosized diol, Lett. Org. Chem. 16 (3) (2019) 235–244.
[7] K. Peng, B.B. Liang, W. Liu, Z.W. Mao, What blocks more anticancer platinum complexes from experiment to clinic: major problems and potential strategies from drug design perspectives, Coord. Chem. Rev. 449 (2021) 214210.
[8] P.K. Kalambate, J. Noiphung, N. Rodthongkum, N. Larpant, P. Thirabowonkitphithan, T. Rojanarata, M. Hasan, Y. Huang, W. Laiwattanapaisal, Nanomaterials-based electrochemical sensors and biosensors for the detection of non-steroidal anti-inflammatory drugs, TrAC, Trends Anal. Chem. 143 (2021) 116403.
[9] F. Dimiza, A. Barmpa, A. Chronakis, A.G. Hatzidimitriou, Y. Sanakis, A.N. Papadopoulos, G. Psomas, Iron (III) complexes with non-steroidal anti-inflammatory drugs: structure, antioxidant and anticholinergic activity, and interaction with biomolecules, Int. J. Mol. Sci. 24 (7) (2023) 6391.
[10] M. Ostadkarampour, E.E. Putnins, Monoamine oxidase inhibitors: a review of their anti-inflammatory therapeutic potential and mechanisms of action, Front. Pharmacol. 12 (2021) 676239.
[11] R. Sánchez-Rodríguez, F. Munari, R. Angioni, F. Venegas, A. Agnellini, M.P. Castro-Gil, A. Castegna, R. Luisetto, A. Viola, M. Canton, Targeting monoamine oxidase to dampen NLRP3 inflammasome activation in inflammation, Cell. Mol. Immunol. 18 (5) (2021) 1311–1313.
[12] V. Tseilikman, E. Dremencov, O. Tseilikman, M. Pavlovicova, L. Lacinova, D. Jezova, Role of glucocorticoid-and monoamine-metabolizing enzymes in stress-related psychopathological processes, Stress 23 (1) (2020) 1–12.
[13] X. Zou, S. Gao, J. Li, C. Li, C. Wu, X. Cao, S. Xia, P. Shao, X. Bao, H. Yang, P. Liu, A monoamine oxidase B inhibitor ethyl ferulate suppresses microglia-mediated neuroinflammation and alleviates ischemic brain injury, Front. Pharmacol. 13 (2022).
[14] A. El Aissouq, O. Chedadi, M. Bouachrine, A. Ouammou, F. Khalil, Development of novel monoamine oxidase B (MAO-B) inhibitors by combined application of docking-based alignment, 3D-QSAR, ADMET prediction, molecular dynamics simulation, and MM_GBSA binding free energy, J. Biomol. Struct. Dyn. (2022) 1–14.
[15] A. Anjum, M.D.I. Yazid, M. Fauzi Daud, J. Idris, A.M.H. Ng, A. Selvi Naicker, O.H.R. Ismail, R.K. Athi Kumar, Y. Lokanathan, Spinal cord injury: pathophysiology, multimolecular interactions, and underlying recovery mechanisms, Int. J. Mol. Sci. 21 (20) (2020) 7533.
[16] K.B. Magalingam, A. Radhakrishnan, N.S. Ping, N. Haleagrahara, Current concepts of neurodegenerative mechanisms in Alzheimer's disease, BioMed Res. Int. 2018 (2018).
[17] W.H. Chuang, Y.T. Chou, Y.H. Chen, T.H. Kuo, W.F. Liaw, T.T. Lu, Y.M. Wang, Neuroprotective effect of NO-delivery dinitrosyl iron complexes (DNICs) on amyloid pathology in the alzheimer's disease cell model, ACS Chem. Neurosci. 14 (16) (2023) 2922–2934.
[18] F. Dimiza, A. Barmpa, A. Chronakis, A.G. Hatzidimitriou, Y. Sanakis, A.N. Papadopoulos, G. Psomas, Iron (III) complexes with non-steroidal anti-inflammatory drugs: structure, antioxidant and anticholinergic activity, and interaction with biomolecules, Int. J. Mol. Sci. 24 (7) (2023) 6391. .
[19] Z. Hazarika, A.N. Jha, Computational analysis of the silver nanoparticle–human serum albumin complex, ACS Omega 5 (1) (2019) 170–178. .
[20] K. Sakthikumar, R.W.M. Krause, B.K. Isamura, A synergistic experimental and structure-based virtual screening, Bioinorgan. Chem. Appl. (2022).
[21] D. Li, B. Zhou, B. Lv, Antibacterial therapeutic agents composed of functional biological molecules, J. Chem. 2020 (2020) 1–13.
[22] A. Muheem, M.A. Jahangir, C.P. Jaiswal, M. Jafar, M.Z. Ahmad, J. Ahmad, M.H. Warsi, Recent patents, regulatory issues, and toxicity of nanoparticles in neuronal disorders, Curr. Drug Metabol. 22 (4) (2021) 263–279. .
[23] E.H. El-Mossalamy, M.E. Batouti, H.A. Fetouh, The role of natural biological macromolecules: deoxyribonucleic and ribonucleic acids in the formulation of new stable charge transfer complexes of thiophene Schiff bases for various life applications, Int. J. Biol. Macromol. 193 (2021) 1572–1586.
[24] R.A. Marcus, Electron transfer reactions in chemistry. Theory and experiment, in: Protein Electron Transfer, Garland Science, 2020, pp. 249–272.
[25] C.K. Moon, J.S. Huh, J.M. Kim, J.J. Kim, Electronic structure and emission process of excited charge transfer states in solids, Chem. Mater. 30 (16) (2018) 5648–5654.
[26] R.S. Almufarij, A.E. Ali, M.E. Elbah, N.S. Hamdy, M.A. Khashaba, H.A. Hamid, H.A. Fetouh, Preparation, characterization of new antimicrobial antitumor hybrid semi-organic single crystals of proline amino acid doped by silver nanoparticles, Biomedicines 11 (2) (2023) 360.
[27] R.S.A. Almufarij, A.E.D. Ali, M.E. Elba, H.E. Okab, O.M. Mailoud, H. Abdel-Hamid, H.A. Fetouh Elsayed, Growth of new, optically active, semi-organic single crystals glycine-copper sulphate doped by silver nanoparticles, Appl. Nanosci. 4 (2) (2023) 115–137.